Available online at www.sciencedirect.com

Manufacturing Letters

Manufacturing Letters 33 (2022) 461–468

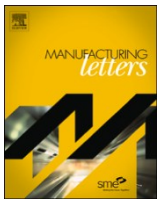

50th SME North American Manufacturing Research Conference (NAMRC 50, 2022)

A preliminary study on improving surface finish of electron beam melted Ti-6Al-4V using piezo vibration striking treatment

Jisheng Chen, Yang Xu, Patrick Kwon, Yang Guo*

Department of Mechanical Engineering, Michigan State University, East Lansing, 48824, MI, USA

* Corresponding author. Tel.: +1-517-432-3164; *E-mail address:* yguo@msu.edu

Abstract

This paper presents an experimental study on surface finish improvement for electron beam melted Ti-6Al-4V using piezo vibration striking treatment (PVST), a novel mechanical surface treatment process realized by a non-resonant piezo stack vibration device installed on a CNC machine. Various experiments with different process parameters, i.e., engagement distance, tool diameter, vibration frequency, and driving voltage, are performed to explore their effects on surface finish of the additively manufactured parts. The results reveal that surface texture after PVST can be divided into two patterns: scattered pattern consisting of scattered treated and untreated areas and uniform pattern with uniform treated areas covered throughout the surface. The compression-type and sliding-type deformation under negative engagement distance between the striking tool and workpiece surface plays an important role in enhancing the surface finish and transforming surface texture from scattered pattern to uniform pattern. Tool diameter, controlling contact area between the tool and the workpiece, is positively correlated with surface finish while driving voltage, controlling vibration amplitude of the tool, is negatively correlated with surface finish. Overlap of indentations controlled by vibration frequency and scan speed has little influence on the surface finish.

Keywords: surface treatment; piezo vibration striking; surface finish; additive manufacturing; process parameters

1. Introduction

The increasing adaptation of additively manufactured (AM) components offers unprecedented design freedom for innovative engineering components and applications in many key industries, such as biomedical, aerospace, energy industries, etc. A wider application of AM metal parts, however, is limited by the poor surface finish, undesirable residual stress, and volumetric defects especially near the surface, which all contributes to the reduced fatigue performance compared to parts manufactured conventionally. Post-processing of the surface is often needed to enhance the finish and mechanical properties of AM metal parts. One common way to do this is by machining such as milling or grinding. Since material removal is involved, this will require the AM parts to be built slightly larger than their original design to accommodate for post-machining. Machining can effectively improve surface finish, but it cannot effectively address the issues of residual stress and subsurface pores. In contrast, mechanical surface treatment uses plastic deformation to modify surface attributes including surface finish, hardness, residual stress, and microstructure. Since material removal is not involved, the AM part does not need to be built oversized. This may lead to cost savings in both build time and materials. More importantly, mechanical surface treatment can effectively generate compressive surface residual stresses, strengthening the surface by strain hardening, and possibly closing the pores beneath the surface. This will greatly benefit the mechanical integrity together with better surface finish and improved fatigue life of AM parts.

In recent years, various mechanical surface treatments have been used to process AM metal parts. Burnishing [1-3]

and deep rolling [4] employ the rolling action of a spherical or cylindrical tool to induce the (continuous) compression-type deformation on part surface. Both have been utilized for the interlayer treatment during the build process in laser powder bed fusion (LPBF) to reduce surface roughness and enhance microstructure and property [5,6]. Shot peening (SP) is the surface treatment in which the surface is stuck by a myriad of small hard steel or ceramic balls energized by compressed air. It has been used to post-process 17-4 stainless steel components fabricated by direct metal laser sintering [7] and AlSi10Mg and Ti6Al4V parts manufactured by selective laser melting (SLM) [8,9]. The results revealed that SP induces more favorable roughness, compressive yield strength, and fatigue resistance. Surface mechanical attrition treatment (SMAT) also is another surface treatment relying on striking the surface. Its difference from SP is that the steel balls are energized by vibration of a closed chamber which contains the loose steel balls and the fixed workpiece. SMAT has been applied on 316L stainless steel parts and Ti-6Al-4V ELI medical components produced by LPBF [10,11] to introduce a nanostructured layer and improve the fatigue performance. Instead of using free indenters, ultrasonic impact peening (UIP) and ultrasonic nanocrystal surface modification (UNSM) [12,13] realizes surface striking by a single tool indenter driven by the ultrasonic actuator and booster. UIP has been applied with directed energy deposition (DED) to enhance fatigue life of in-situ processing Inconel 718 [14]. UNSM has been used to process Ti-6Al-4V and AISI 316L made by DED [15,16]. It was found that UNSM resulted in a better surface finish and lower subsurface porosity.

The vibration-based striking surface treatment such as UIP and UNSM have the advantage to be easily implemented on a computer numerical control (CNC) machine which enables more precise control on the striking location and treated area, and better automation of the treatment process. However, ultrasonic vibration is dependent on the resonance of the vibrating structure, so its frequency and amplitude cannot be varied and controlled easily [17]. This characteristic has limited the ability of UIP and UNSM to control the striking intensity and the resulting surface deformation during the treatment process. Compared with ultrasonic vibration, the non-resonant mode piezo vibration is more convenient to control in both amplitude and frequency. This has led to the recent development of piezo vibration striking treatment (PVST) [18]. Previous study has shown that PVST has good controllability over each individual strike and is capable of creating different surface texture on an originally smooth surface. The present study is focused on how to apply PVST to efficiently improve surface finish of selective E-beam melted Ti-6Al-4V.

2. Experimental Setup

The experimental setup of PVST is shown in Fig. 1. PVST device is connected to the spindle of a CNC mill (Hass VF-4) through a standard CAT40 tool holder. During the treatment, the spindle rotation is locked; the PVST device controls the tool vibration while the CNC machine controls the tool feed motion in X, Y and Z directions. The horizontal tool feed motion is also referred to as tool scan motion.

Figure 1b shows the schematic of the PVST device. Inside the device body, a non-resonant piezo stack actuator is assembled with a spline shaft nested in a ball spline bearing along the axial direction. The spline bearing allows only linear motion of the shaft along the axial direction since bending and rotation are restricted. The cylinder striking tool has a hemispherical end and is made of M2 high-speed steel. It is rigidly connected to the shaft through a tool holder. A function generator together with a power amplifier produces the sinusoidal driving voltage to control the extension and contraction of the piezo stack and hence actuate the tool vibration. The vibration amplitude is proportional to the driving voltage amplitude. The maximum peak-to-peak voltage amplitude is V_{pp} = 150 V, which corresponds to the peak-to-peak vibration amplitude of u_{pp} = 100 μm.

Figure 1c illustrates the linear tool scan path used in PVST. Each cycle of tool vibration will result in one strike on the

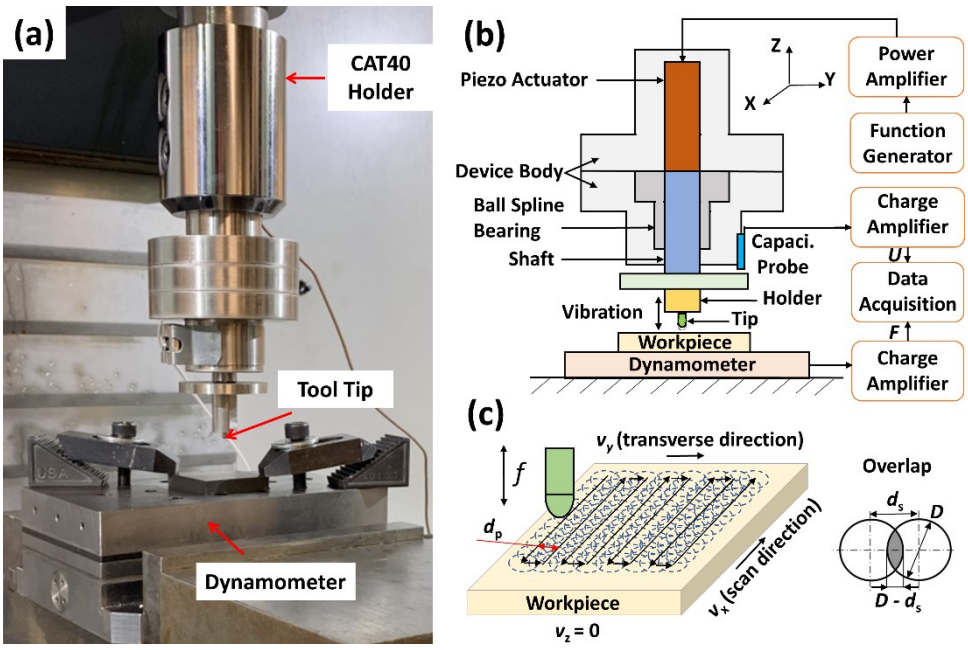

Figure 1 (a) The real picture (b) the schematic illustration of PVST and (c) the schematic illustration of surface texture after PVST.

surface. The successive strikes will have a constant spacing (d_s) along the scan direction which is dependent on the scan speed (v_s) and the vibration frequency (f) as $d_s = v_s / f$. The overlap ratio (r_o) between two successive strikes can be defined as $r_o = (D - d_s) / D$ (see Fig. 1c), where D is the diameter of the indentation created by a single strike. Likewise, the spacing between two scan lines (d_p) controls the overlap ratio in the transverse direction (normal to scan line). In this study, d_p will be kept the same as d_s for each treatment condition in the study.

PVST experiments were conducted on selective electron beam melted Ti-6Al-4V with a build dimension of 110 mm × 12 mm × 3 mm. The treated area for each treatment condition is 5 mm × 5 mm. Surface 3D topography and roughness values (R_a, R_z, and S_a) of the treated areas were measured using KEYENCE Digital Microscope (VHX-6000).

3. Results and Discussion

Figure 2 compares the roughness layer of the initial workpiece surface with the roughness layers of the treated surfaces after PVST. The roughness S_a of the initial surface whose rough features are scattered throughout the area is 28.6 µm (Fig. 2a). The treated surfaces after PVST show reduced surface roughness, as shown in Fig. 2b (S_a = 16.3 µm) and 2c (S_a = 8.3 µm). The roughness layer in Fig. 2b consists of scattered dark and bright areas. The bright areas represent the impacted areas that interact with the striking tool while the dark areas are the unaffected areas that cannot be approached by the tool. The roughness layer in Fig. 2c is covered by uniform bright areas with only a few dark hills or valleys. The surface height maps also show smoother characteristics in Fig. 2b and 2c than in Fig. 2a. This paper distinguishes the surface after PVST into two patterns: the scattered and uniform patterns. The scattered pattern is used to represent the roughness layer consisting of the scattered dark and bright areas and the uniform pattern to the roughness layer covered by uniform bright areas.

3.1. Effect of Engagement Distance on Surface Deformation

In PVST, the nominal stroke of the piezo stack actuator is 100 µm under the maximum driving voltage (V_{pp} = 150 V). During the striking process, the vibration amplitude reduces because of the elastic compression of the device assembly under the striking force. To accommodate the vibration range and amplitude reduction and achieve a better surface finish, the engagement distance (Z) between the striking tool and the workpiece surface should be selected properly.

Figure 3 illustrates the possible interactions between the vibration tool and the rough surface layer in PVST of AM part. The reference for Z is defined as the highest feature of the surface layer. In Fig. 3a, the tool and the surface have a positive engagement distance ($Z > 0$), i.e., the tool is above the surface at its minimum vibration displacement. In this case, the vibration amplitude needs to be larger than the engagement distance ($u_{pp} > Z$) to induce the strikes on the surface layer, and the effective vibration amplitude is actually $u_{pp} - Z$, indicating that the vibration amplitude u_{pp} is not fully utilized. Each tool vibration leads to one strike on the roughness features. The induced deformation is more of a compression type, whose effect would be flattening the hills of the roughness features. The valleys of roughness features beyond the reach of the tool will likely be unaffected. For the rougher surface with a high peak-to-valley roughness value (R_z), a larger vibration amplitude is needed for the tool to reach the bottom of the roughness layer. Since the measured average R_z throughout the treated area of the workpiece is about 140 µm (> nominal stroke of the actuator), the striking tool is unable to reach the bottom

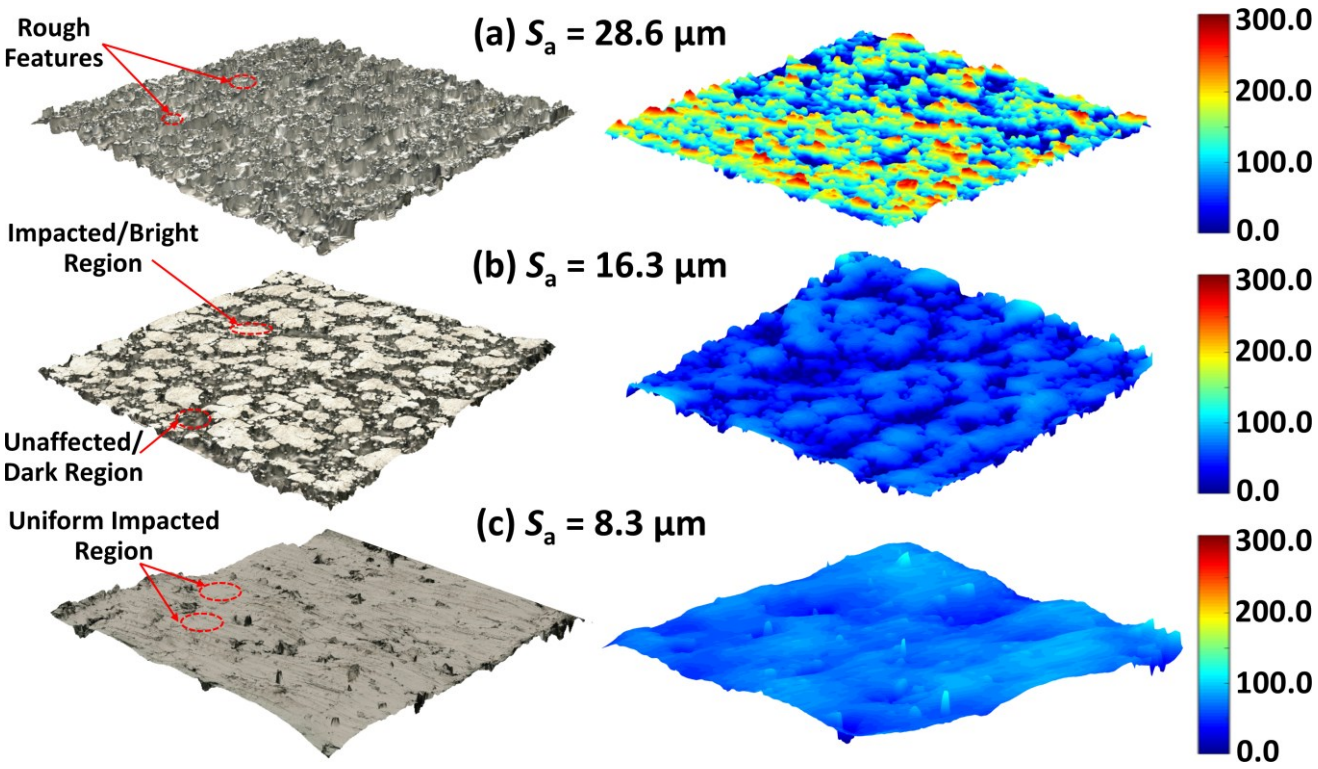

Figure 2 Surface textures and surface height maps: (a) the initial surface pattern; (b) the scattered pattern; (c) the uniform pattern.

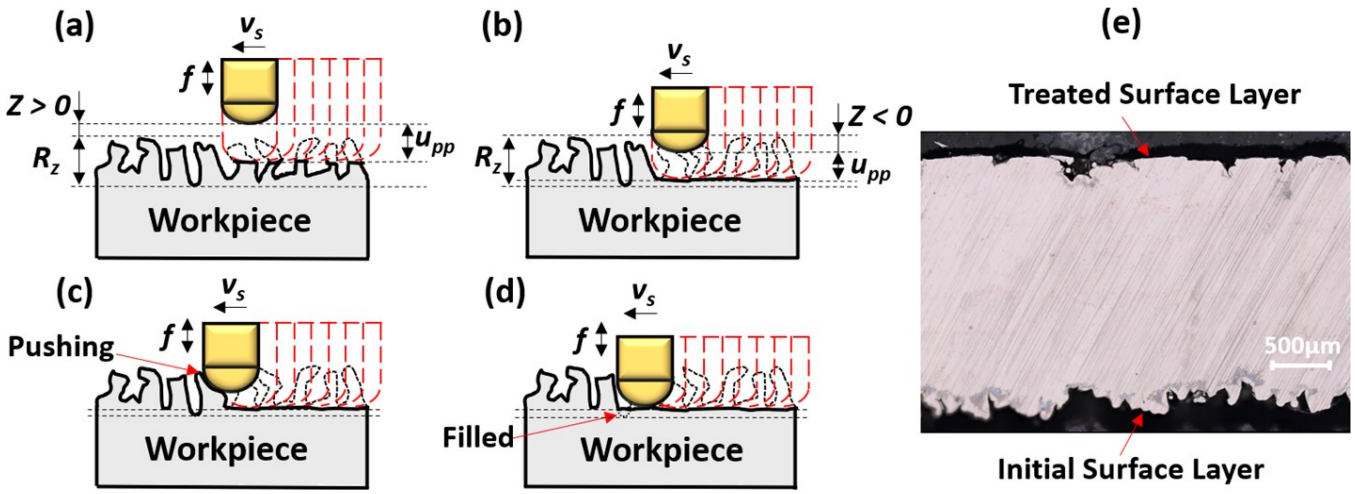

Figure 3 (a) – (d) The schematic illustration of tool engaging process; (e) The cross-section of the treated workpiece after PVST.

of the roughness layer in the current setting or even though Z is set as 0. Therefore, the compression and flattening effect on the roughness features cannot be thoroughly realized at $Z > 0$. In Fig. 3b - 3d, the tool and the workpiece surface have a negative engagement distance ($Z < 0$), i.e., the tool is penetrating the roughness layer even at its minimum vibration displacement position. The tool is always engaged with the rough surface during its full vibration amplitude range. The required vibration amplitude to reach the bottom of the roughness layer is significantly reduced. In this case, besides compression-type deformation (Fig. 3b), the tool will also induce sliding-type deformation (Fig. 3c) due to the tool horizontal scan at a negative engagement distance. The sliding-type deformation is likely to be more effective in displacing the material from the hills to the valleys for the highly rough surface (Fig. 3d). Figure 3e illustrates the cross-section profiles of the workpiece before (lower surface) and after (upper surface) PVST measured using KEYENCE Digital Microscope. It is observed that the roughness hills are flattened by the tool and no voids or cracks exist on the flattened area compared to the initial rough surface profiles, showcasing the enhanced effect of flattening-sliding deformation on the roughness layer. Some micro-cracks and voids on the bottom of the roughness layer are still observed due to the limited striking depth, which could be eliminated with a smaller Z or larger u_{pp}.

To investigate the effect of Z on the surface roughness, different Z values (Z = -50, -80, -110, and -140 μm) are selected under the condition of f = 100 Hz, V_{pp} = 150 V, v_s = 750 mm/min, d = 3 mm (tool diameter). It is observed in Fig. 4a the bright areas increase as Z decreases, indicating more interaction between the tool and the rough surface. The uniform pattern is observed at Z = -140 μm while the scattered pattern is seen in other conditions. Figure 4b and 4c summarize the quantified roughness parameters (S_a, R_a, and R_z) for these surfaces. The one-dimensional roughness parameters (R_a and R_z) are measured along both the scan and the transverse directions. It demonstrates that the roughness parameters are consistent with the corresponding surface textures shown in Fig. 4a; the roughness parameters decrease as Z is reduced. Both R_a and R_z are statistically the same along the scan direction and the transverse direction. S_a has similar value as R_a for all the conditions. The smallest S_a obtained at Z = -140 μm is 9.3 μm, which is smaller than the initial surface roughness (S_a = 28.6 μm) by 67.5%.

For the AM parts with high roughness features, it is difficult to maintain a constant vibration amplitude during the treatment due to the high unevenness, so the selection of Z value should be able to tackle the varied vibration amplitude

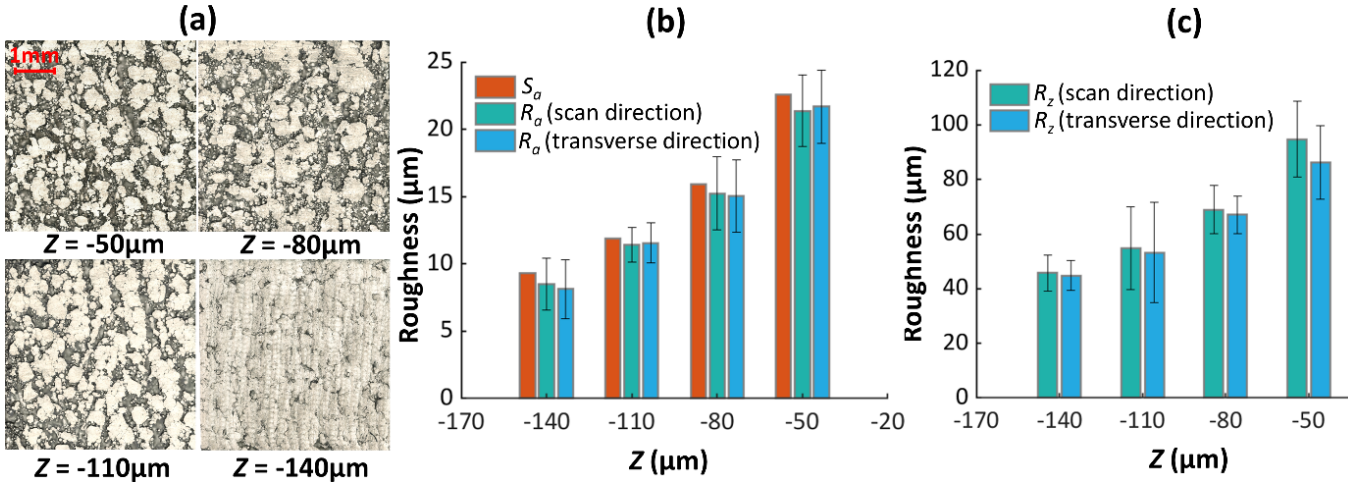

Figure 4 (a) Surface textures after PVST under different Z values; (b) and (c) the relationships of the roughness parameters (S_a, R_a, R_z) with Z.

and get a smooth surface. The above results show that it is good practice to use -R_z as the starting Z value to determine the engagement distance between the striking tool and the workpiece surface. In some cases, it may be necessary to use a smaller Z than -R_z to realize the flattening-sliding effect more thoroughly since R_z is a one-dimensional approximation of the peak-to-valley roughness throughout the target area and might not perfectly represent those surfaces with high roughness features.

3.2. Effect of Tool Diameter on Surface Deformation

The diameter (d) of the striking tool influences the surface deformation by changing the contact area between the striking tool and the workpiece in PVST. The schematic in Fig. 5a shows the interaction between the striking tool and the workpiece surface in a single strike which forms the indentation with the depth h and the width W. Larger h and smaller W can be achieved by decreasing d while keeping other experimental parameters constant as smaller d leads to less contact area and hence less deformation resistance. This enables the tool to reach a deeper position of the roughness layer, which has been verified in the experiments under the conditions of f = 100 Hz, V_{pp} = 150 V, d = 2, 3, and 4 mm, v_s = 750 mm/min, and Z = -140 µm.

As illustrated in Fig. 5a, the uniform pattern occurs at d = 2 mm and d = 3 mm while the scattered pattern occurs at d = 4 mm where the dark areas increase significantly. The higher deformation resistance caused by the larger tool diameter leads to larger elastic compression on the vibration device assembly which reduces the maximum tool displacement during the vibration. Therefore, the tool cannot reach the bottom of the roughness layer, leaving more areas unaffected. In addition, the roughness parameters in Fig. 5b and 5c are in good agreement with the surface textures shown in Fig. 5a. All the roughness parameters at d = 4 mm are larger than those at d = 2 mm and d = 3mm, and the maximum difference of S_a is about 6 µm. The roughness parameters at d = 3 mm are slightly larger than those at d = 2mm, which are consistent with the uniform pattern exhibited in Fig. 5a. It is observed that R_z in the transverse direction is larger than R_z in the scan direction by ~18 µm at d = 4 mm. This difference might be caused by the continuous dark areas band at the top of the treated surface (along the horizontal/transverse direction), which contributes to a larger R_z value in the transverse direction.

For a uniform or low roughness surface, the striking tool should be able to approach the lowest valley of the roughness layer at Z = -R_z regardless of the variation of d. Because the vibration amplitude cannot reduce to zero, and a small amount of vibration amplitude will make the strikes reaching the bottom of the roughness layer possible. However, this might not be the case for a non-uniform surface. Owing to the unevenness of the roughness layer, the roughness height may differ at distinct locations throughout the layer. In this case, the average R_z could not perfectly reflect the distance between the highest hill and the lowest valley throughout the roughness layer. When using the striking tool with a large diameter, the increasing contact area and corresponding deformation resistance will further decrease the vibration amplitude and prevent the striking tool from approaching the bottom of the roughness layer. Therefore, the striking depth at d = 4 mm is smaller than that at d = 2 mm and d = 3 mm, resulting in the scattered pattern of surface texture. Under the circumstances, a smaller Z can be used to balance the reduction of the vibration amplitude in large diameter conditions, which will be validated in future work.

3.3. Effect of Driving Voltage on Surface Deformation

The vibration amplitude of the striking tool is controlled by the amplitude of the driving voltage V_{pp}. Higher driving voltage can generate higher dynamic energy and hence higher vibration amplitude. Thus, the tool can be extended more to strike a deeper position of the roughness layer, thereby enhance the flattening-sliding effect to improve the surface finish.

Figure 6 compares the surface textures and roughness parameters achieved under different driving voltage conditions (V_{pp} = 50, 100, 150 V, f = 100 Hz, d = 2 mm, v_s = 450 mm/min) at Z = -140 µm and Z = -110 µm. More scattered bright areas are observed in Fig. 6a as V_{pp} increases from 50 V to 150 V, and the surface texture transforms from the scattered pattern to the uniform pattern when V_{pp} reaches 150 V both at Z = -140

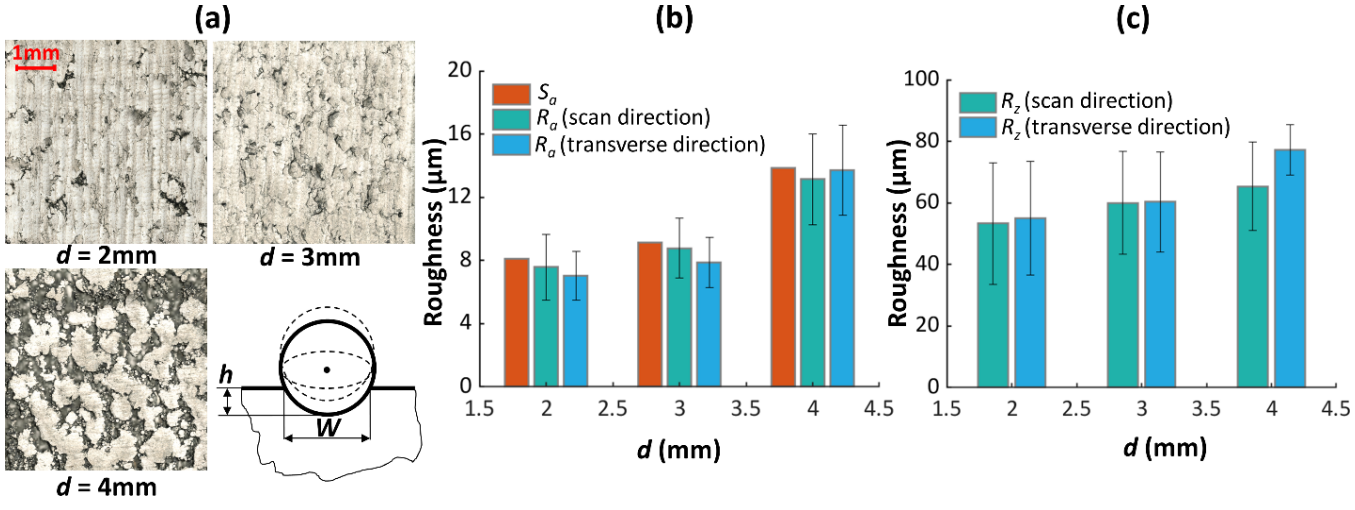

Figure 5 (a) Surface textures after PVST under different tool diameters; (b) and (c) the relationships of the roughness parameters (S_a, R_a, R_z) with tool diameter.

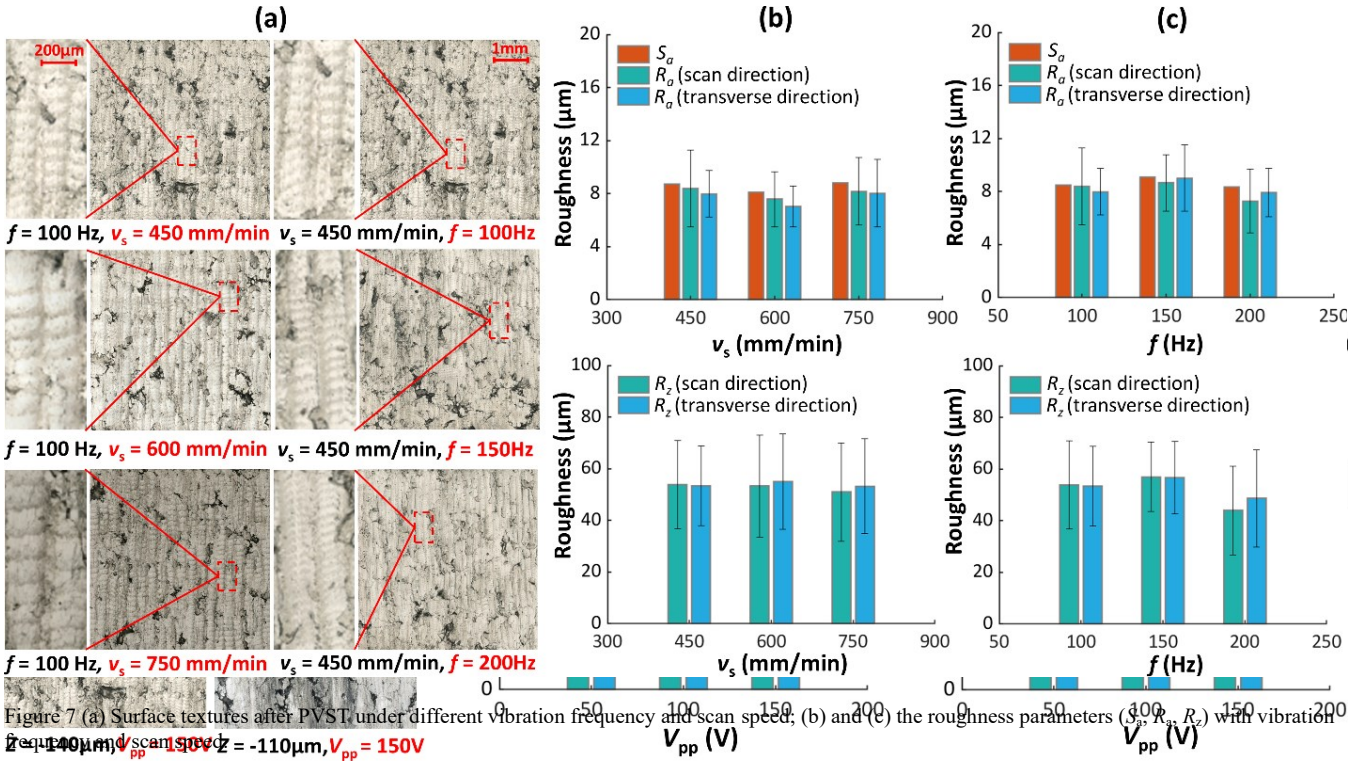

Figure 7 (a) Surface textures after PVST under different vibration frequency and scan speed; (b) and (c) the roughness parameters (S_a, R_a, R_z) with vibration frequency and scan speed.

Figure 6 (a) Surface textures after PVST under different driving voltages at Z = -140 μm and Z = -110 μm; (b) and (c) the relationships of the roughness parameters (S_a, R_a, R_z) with driving voltage.

μm and Z = -110 μm. There are more dark areas scattered at Z = -110 μm for all the voltage conditions compared to those at Z = -140 μm. This is caused by the smaller striking depth of the tool with a larger (or less negative) Z which results in more unapproached areas. The roughness parameters in Fig. 6b and 6c are negatively correlated with the driving voltage. S_a and R_a at Z = -110 μm are larger than that at Z = -140 μm for all the driving voltage conditions while R_z at Z = -140 μm is close to that at Z = -110 μm. These results are consistent with the surface textures demonstrated in Figure 6a where higher driving voltages produce more bright areas and smoother surface features.

3.4. Effect of Indentation Overlap on Surface Deformation

As mentioned in Fig. 1c, the overlap ratio r_o is inversely proportional to v_s and proportional to f, indicating that higher vibration frequency and lower scan speed can result in denser distribution of the indentations with the same treated size. This is beneficial for surface finish enhancement, so a combination of high vibration frequency and low scan speed would be a great choice to perform PVST under the ideal circumstance. Yet, lower scan speed requires longer processing time and higher frequency requires a more powerful actuation source, which may be time-consuming and costly. Therefore, how to trade off these factors is of great significance to implement a more economical and efficient PVST.

To study the effect of the overlap of the indentations on the surface deformation, various experiments are performed by varying f (f = 100 - 200 Hz, v_s = 450 mm/min) and v_s (v_s = 450 - 750 mm/min, f = 100 Hz) under the condition of d = 2 mm, Z = -140 μm, and V_{pp} = 150 V. As shown in Fig 7a, the surface textures in all the conditions present the uniform pattern thanks to the use of small tool diameter (d = 2 mm) and large negative engagement distance (Z = -140 μm). The successive indentations along the scan direction can be clearly observed in all the conditions, which are absent on the surface textures with the scattered pattern. When v_s decreases from 750 mm/min to 450 mm/min, the distribution of the indentations becomes denser, showing the rectangle-like features on the treated surface. Likewise, when f increases from 100 Hz to 200 Hz, the denser distribution of the indentations is observed. At f = 200 Hz, the surface textures present line-like features caused by the highly dense overlap of the indentations since higher frequency enables the tool to strike the surface with more strikes at a certain area. Moreover, due to the nonuniform roughness layer, part of intrinsic defects, such as voids and cracks, cannot be eliminated thoroughly, leading to a few dark areas distributed on the treated surface.

Figures 7b and 7c summarize the roughness parameters under different scan speeds and vibration frequencies. It is seen in Fig. 7b the roughness values (S_a, R_a, and R_z) are not affected too much by the scan speed and are consistent with surface textures with the uniform pattern. These results are different from those metal parts with an initial smooth surface where the surface roughness decreases with lower scan speed [18]. The improvement in AM parts under different scan speeds after PVST may be balanced by those rough untreated areas when calculating the roughness parameters throughout the treated surface, thereby leading to similar roughness parameters for different scan speeds. Moreover, it takes 45 s, 26 s, and 17 s at v_s = 450, 600, and 750 mm/min to process a targeted area of 5 mm × 5 mm in PVST, respectively. Based on the roughness results and the processing time, v_s = 750 min/min would be a more efficient choice than v_s = 450 min/min or v_s = 600 min/min. Similarly, the roughness parameters in Fig. 7c illustrate that the vibration frequency does not influence the surface roughness significantly due to the non-uniform surface

characteristics. Although fewer dark areas and smaller R_z values are observed at f = 200 Hz, which should make the surface smoother, the overall roughness parameters are still close to the other two conditions.

Consequently, the above results reveal that the overlap of the indentations does not exert a considerable influence on the overall surface roughness of AM metal parts. Based on the requirements of surface roughness and processing efficiency, a combination of v_s = 750 mm/min and f = 100 Hz is sufficient to achieve the equivalent surface roughness using PVST.

4. Conclusions

This study has experimentally explored the non-resonant PVST emphasizing the surface textures and surface finish of AM metal parts. It can be concluded that:

- PVST can induce surface plastic deformation to improve the surface finish at different levels by controlling process parameters.
- Two surface texture patterns are found and affected by the treatment level: the scattered pattern consisting of scattered treated and untreated areas, and the uniform pattern with uniform treated areas throughout the surface.
- Negative Engagement distance is important to apply compression-type deformation and sliding-type deformation simultaneously. To achieve the uniform pattern, the engagement distance should be negative enough to enable the tool to reach the bottom of the roughness layer. The peak-to-valley roughness can be used as a starting engagement distance to achieve the uniform surface texture.
- Smaller tool diameter and higher drive voltage are beneficial to improve the surface finish and easier to realize the uniform pattern surface texture.
- Varying vibration frequency and scan speed changes the overlap of the indentations. But the overlap does not have a significant effect on the surface finish improvement. The selection of vibration frequency and scan speed should take into consideration the processing time and vibration energy consumption.

Acknowledgements

This work is supported by NSF CMMI grant no. 2019320.

References

[1] V.P. K., S.Yu. T., A.I. D. Nanostructuring burnishing and subsurface shear instability. J Mater Proc Tech 2016; 217:327–335.

[2] Michela S., Giovanna R., Maria Rosaria S., Luigino F. Burnishing of AM Material to Obtain High Performance Part Surfaces. J Indus Eng Manage 2022; 15(1):73–89.

[3] R. K., P. Vijay A., C. K., C. K., Adwait J., Shrikant J., A. S. S. B. Exploring grinding and burnishing as surface post-treatment options for electron beam additive manufactured Alloy 718. Surf Coat Tech 2020; 397:126063.

[4] Berend D., Alexander K., Steffen H., Kolja M., Philipp P. Surface topography after deep rolling with milling kinematics. Prod Eng 2021; 15:327–333.

[5] Sumair S., Ritin M., Haoliang Y., Arif M. Effects of microstructure and inherent stress on residual stress induced during powder bed fusion with roller burnishing. J Mech Sci 2022; 219:107092.

[6] Daniel M., Nicole W. Internal reinforced domains by intermediate deep rolling in additive manufacturing. Manu Tech 2019; 68:519–582.

[7] AlMangour B., and Yang J. M. Improving the Surface Quality and Mechanical Properties by Shot-Peening of 17-4 Stainless Steel Fabricated by Additive Manufacturing. Mater Des 2016;110:914–924.

[8] Uzan N. E., Ramati S., Shneck R., Frage N., and Yeheskel O. On the Effect of Shot-Peening on Fatigue Resistance of AlSi10Mg Specimens Fabricated by Additive Manufacturing Using Selective Laser Melting (AM-SLM). Addit Manuf 2018; 21:458–464.

[9] Slawik S., Bernarding S., Lasagni F., Navarro C., Periñán A., Boby F., Migot-Choux S., Domínguez J., and Mücklich F. Microstructural Analysis of Selective Laser Melted Ti6Al4V Modified by Laser Peening and Shot Peening for Enhanced Fatigue Characteristics. Mater Charact 2021; 173:110935.

[10] Yan X., Yin S., Chen C., Jenkins R., Lupoi R., Bolot R., Ma W., Kuang M., Liao H., Lu J., and Liu M. Fatigue Strength Improvement of Selective Laser Melted Ti6Al4V Using Ultrasonic Surface Mechanical Attrition. Mater Res Lett 2019;7(8):327–333.

[11] Portella Q., Chemkhi M., Retraint D. Influence of Surface Mechanical Attrition Treatment (SMAT) Post-Treatment on Microstructural, Mechanical and Tensile Behaviour of Additive Manufactured AISI 316L. Mater Charact 2020; 167:110463.

[12] Cao X. J., Pyoun Y. S., Murakami R. Fatigue Properties of a S45C Steel Subjected to Ultrasonic Nanocrystal Surface Modification. Appl Surf Sci 2010; 256(21):6297–6303.

[13] Amanov A., Cho I. S., Pyoun Y. S., Lee C. S., Park I. G. Micro-Dimpled Surface by Ultrasonic Nanocrystal Surface Modification and Its Tribological Effects. Wear 2012; 286:136–144.

[14] Wang Y., Shi, J. Microstructure and Properties of Inconel 718 Fabricated by Directed Energy Deposition with In-Situ Ultrasonic Impact Peening. Metall Mater Trans B 2019; 50(6):2815–2827.

[15] Zhang H., Chiang R., Qin H., Ren Z., Hou X., Lin D., Doll G. L., Vasudevan V. K., Dong Y., Ye C. The Effects of Ultrasonic Nanocrystal Surface Modification on the Fatigue Performance of 3D-Printed Ti64. Int J Fatigue 2017;103:136–146.

[16] Kim M.-S., Jo Y. K., Park S. H., Shim D. S. Application of Ultrasonic Nanocrystal Surface Modification for Improving Surface Profile of DEDed AISI 316L. J Mech Sci Technol 2019;33(12):5659–5667.

[17] Altintas Y. Manufacturing Automation: Principles of Metal Cutting and Machine Tool Vibrations. Cambiridege: Cambridge University Press; 2000.

[18] Jisheng C., Yang X., Juan S., Patrick K., Yang G. On Force-Displacement Characteristics and Surface Deformation in Piezo Vibration Striking Treatment. J Manuf Sci Eng Trans ASME 2022; 144(6):061011.